Enhancing Li-ion Transport in Solid Electrolytes by Confined Water

Yutong Li, Shitong Wang, Jin Leng, Zunqiu Xiao, Zhongtai Zhang, Tao Gao, and Zilong Tang**

Dr. Y. Li, J. Leng, Z. Xiao, Prof. Z. Zhang, Prof. Z. Tang
State Key Lab of New Ceramics and Fine Processing
School of Materials Science and Engineering
Tsinghua University
Beijing 100084, P. R. China
Email: tzl@tsinghua.edu.cn

Dr. Y. Li,
College of New Energy
China University of Petroleum (East China)
Qingdao 266580, P. R. China

Dr. S. Wang, Prof. T. Gao
Department of Chemical Engineering
The University of Utah
Salt Lake City, UT 84112, USA
Email: taogao@chemeng.utah.edu

Dr. S. Wang
Department of Nuclear Science and Engineering
Massachusetts Institute of Technology
Cambridge, MA 02139, USA

Developing new oxide solid electrolytes with fast Li-ion transport and high stability is an important step to realize high-performance solid-state Li-ion batteries. Hydrates materials containing confined water widely exist in nature or can be easily synthesized. However, they have seldom been explored as Li solid electrolytes due to the stereotype that the presence of water limits the electrochemical stability window of a solid electrolyte. In this work, we demonstrate that confined water can enhance Li-ion transport while not compromising the stability window of solid electrolytes using Li-H-Ti-O quaternary compounds as an example system. Three Li-H-Ti-O quaternary compounds containing different amounts of confined water were synthesized, and their ionic conductivity and electrochemical stability are compared. The compound contains nano-confined pseudo-water is demonstrated to have an ionic conductivity that is 2~3 order of magnitude higher than the water-free $Li_4Ti_5O_{12}$ and similar stability window. A solid-state battery is made with this new compound as the solid electrolyte, and good rate and cycling performance are achieved, which demonstrates the promise of using such confined-water-containing compounds as Li-ion solid electrolytes. The knowledge and insights gained in this work open a new direction for designing solid electrolytes for future solid-state Li-ion batteries. Broadly, by confining water into solid crystal structures, new design freedoms for tailing the properties of ceramic materials are introduced, which creates new opportunities in designing novel materials to address critical problems in various engineering fields.

1. Introduction

Li-ion batteries (LIBs) have revolutionized the portable electronics industry and are transforming our transportation by electrifying vehicles. As one of the most important components in a LIB, the electrolyte is key to LIB's power performance, durability, and safety. Despite liquid electrolytes being mostly used in LIBs, in recent years solid electrolytes (SEs) emerge as promising due to their intrinsic non-flammability and better thermodynamic stability[1]. The ion transport property of SEs, characterized by ionic conductivity or diffusivity, is one of the most important features of SEs because it governs the power performance and energy efficiency of solid-state LIBs. Another important property of SEs is their electrochemical stability window, which determines the voltage, therefore power and energy density of LIBs.

Several classes of Li-ion SEs have been developed in the past decades, including oxides, sulfides, polymer, and oxide-polymer composites[2] (Table S1, Supporting Information). Among them, oxides are especially attractive because they have a good balance between high Li-ion conductivity and wide electrochemical stability window[3]. However, their Li-ion conductivity (10^{-3}~10^{-8} S cm^{-1}) is still much lower than that of liquid electrolytes (~10^{-2} S cm^{-1}). To address this challenge, various strategies have been proposed to increase the ionic conductivity of oxide SEs. The most common one is structural engineering by elemental substitution, including both cation substitution and anion substitution[3-4]. For example, many researchers try to substitute La^{3+} and/or Ti^{4+} in $Li_{3x}La_{2/3-x}\square_{1/3-2x}TiO_3$ (LLTO)[3]. However, most substitution shows minimal enhancement of Li-ion conductivity except for the substitution of Ti^{4+} with Al^{3+}, Ge^{4+} [3]. In contrast, replacing O with larger and more polarizable anions (e.g., S) has been proven to be more effective because the high polarizability of anion weakens interactions of Li^+ with the anionic sub-lattice[5]. For example, Kanno first reported the enhancement of Li-ion conductivity for LiSICONs SEs by replacing O with S[6]. This discovery triggers an intensive study of sulfides-based SEs[7], resulting in a Li-ion conductivity comparable to that of liquid

electrolytes (up to 10^{-2} S cm^{-1})[2-3]. However, the intrinsically low electrochemical stability window (0.3~0.6 V) of sulfide SEs constrains their application in LIBs[8]. Therefore, the research efforts in modifying existing oxide SEs have shown limited progress. Designing new oxide SE materials is highly essential to the success of solid-state LIBs.

Many materials, such as minerals[9], clays[10], gels[11], gelatins[12], contain confined water in the structure. Fundamentally, confined water includes nano-confined water (also termed as crystallization water[13]) and nano-confined pseudo-water, which are HO species whose H:O stoichiometry is not 2:1, such as –OH group, hydroxide, and hydronium[14]. In our previous study, we accidentally found the confined-water-containing $Li_{1.25}H_{1.63}Ti_2O_{5.44-\sigma}$ has a lithium diffusion coefficient 3~5 orders of magnitude higher than the confined-water-free $Li_4Ti_5O_{12}$-TiO_2[15]. Such a discovery suggests that the Li-ion transport in oxide SEs can be enhanced by confined water in the crystal structure (**Figure 1**). This work aims to test this hypothesis by studying how confined water affects the performance of Li-H-Ti-O quaternary compounds as SE. Li-H-Ti-O compounds with different amounts of confined water are first synthesized, then their Li ion conductivity and stability are characterized. Lastly, Li-ion batteries based on these compounds as SEs are made and the electrochemical performance is examined.

2. Results

Materials containing confined water can be easily synthesized via hydrothermal[16] or sol-gel[17] methods, and the confined water can be removed by thermal treatment. Typically, the weight loss occurs in stages (Figure 1a), and three types of water exist based on the differences in the activation energy[14, 18] (Table S2, Supporting Information). They are 1) surface-adsorbed water[18-19], 2) nano-confined water[14, 20], which is water molecule that constitutes the crystal structure, and 3) nano-confined pseudo-water[14, 20a, 21], which is hydrogen-containing species with an H:O stoichiometry other than 2:1, such as –OH group [15, 22], hydroxide[23] and hydronium[14, 24] (Figure 1c). Here H-Ti-O

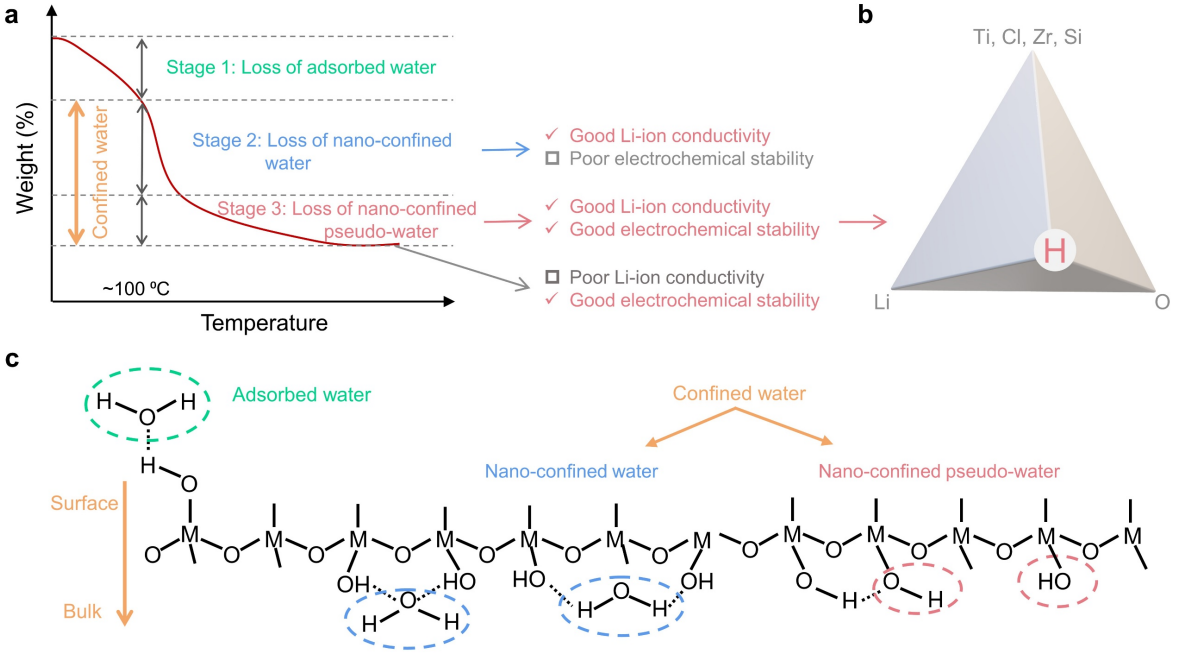

Figure 1. Illustration of confined water in solids. a) Loss of different hydrogen-containing species in solids under increasing temperature, b) quaternary phase diagram with confined water, c) schematic of three types of hydrogen species in solids.

compound containing a large amount of confined water is first synthesized via hydrothermal reaction, resulting in a layered structure (denoted as HTO, Figure S1, Supporting Information). Then a Li-H-Ti-O layered structure (denoted as LHTO-pre) was obtained by an ionic exchange treatment of HTO in a LiOH solution. Finally, LHTO-pre is heat-treated at a low temperature (200 °C). At this temperature, all the surface-adsorbed water and part of nano-confined water can be removed. The resulted compound is denoted as LHTO. The weight loss of this process is illustrated in **Figure 2**a. According to thermogravimetry analysis (TGA) and elemental analysis, the chemical formulars of LHTO-pre and LHTO are determined as $Li_{1.81}H_{0.19}Ti_2O_5 \cdot H_2O$, and $Li_{1.81}H_{1.13}Ti_2O_{5.15-\sigma}$, respectively. The phase transformation of LHTO-pre during the dehydration process is further studied by X-ray diffraction (XRD) (Figure 2b). When the temperature is increased to 200 °C, a possible intermediate phase (LHTO) appears with decreased interlayer spacing from 0.8 nm to 0.6 nm (Figure S2, Supporting Information). FTIR shows hydrogen exists mainly in the form of Ti–OH (Figure S3, Supporting Information), confirming the presence of nano-confined pseudo-water. Scanning electron microscopy (SEM) images show the LHTO-pre has a nanowire morphology, which is maintained during the heat-treatment at 200 °C (Figure 2c, e). High-resolution transmission electron microscopy (HRTEM) (Figure 2d, f) images show more lattice distortion and defects appearing in LHTO than LHTO-pre, which would benefit the Li-ion transport[25]. Further increasing the temperature leads to the loss of all confined water (Figure 2a) and the collapse of the layered structure. XRD shows the sharp peaks

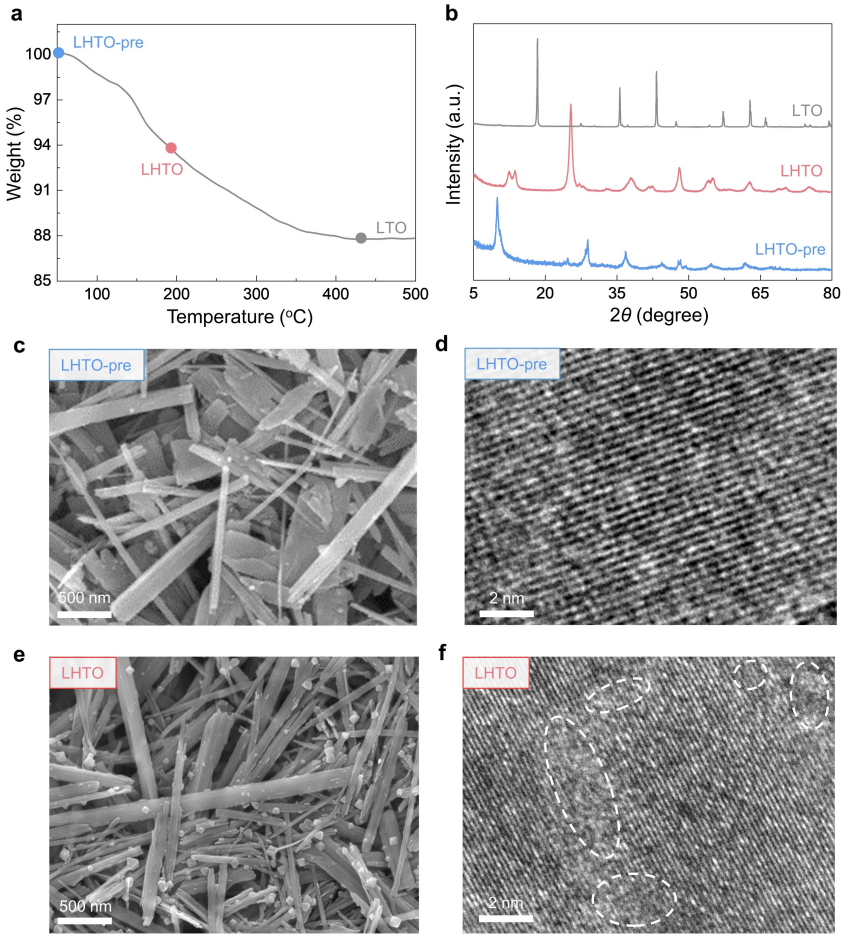

Figure 2. Structural characterization of the synthesized Li-H-Ti-O quaternary compound. a) TGA of LHTO-pre, b) XRD of LHTO-pre, LHTO and LTO, c) SEM and d) HRTEM of LHTO-pre, e) SEM and f) HRTEM of LHTO.

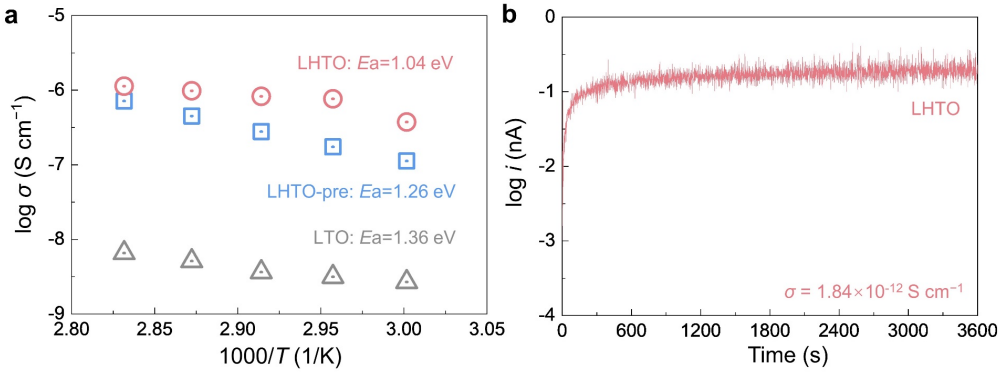

Figure 3. Kinetics study of the synthesized Li-H-Ti-O quaternary compound. The conductivity of a) Li^+ and b) e^-.

associated with the high-temperature $Li_4Ti_5O_{12}$ phase (LTO, Figure 2b) and the amorphous-glassy phase disappears (Figure S4, Supporting Information).

To examine the conductivity of the synthesized Li-H-Ti-O ternary compounds containing different amounts of confined water, the LHTO-pre, LHTO, and LTO powders are first cold-compressed into pellets in a die (Figure S5, Supporting Information). To measure the Li^+ conductivity, a Li|PEO|pellet|PEO|Li sandwich cell is made, and then direct current (DC) measurement is performed with the same cell at different temperatures between 60 °C to 80 °C. The result shows the Li-ion conductivities of LHTO-pre and LHTO at 60 °C are 1.12 $\times 10^{-7}$ S cm^{-2} and 3.74 $\times 10^{-7}$ S cm^{-2}, respectively, which is 2 orders of magnitude higher than that of the water-free LTO (2.68 $\times 10^{-9}$ S cm^{-2}) (**Figure 3**a). To measure the electronic conductivity of the sample, an ss|pellet|ss sandwich cell is made (ss refers to stainless steel) for DC measurement. The result shows the electronic conductivity of LHTO is about ~10^{-12} S cm^{-2} (Figure 3b), which is 5 orders of magnitude lower than its ionic conductivity. These results confirm the suitability of LHTO as a SE. Its conductivity is comparable to amorphous LiPON or solid polymer electrolytes[26].

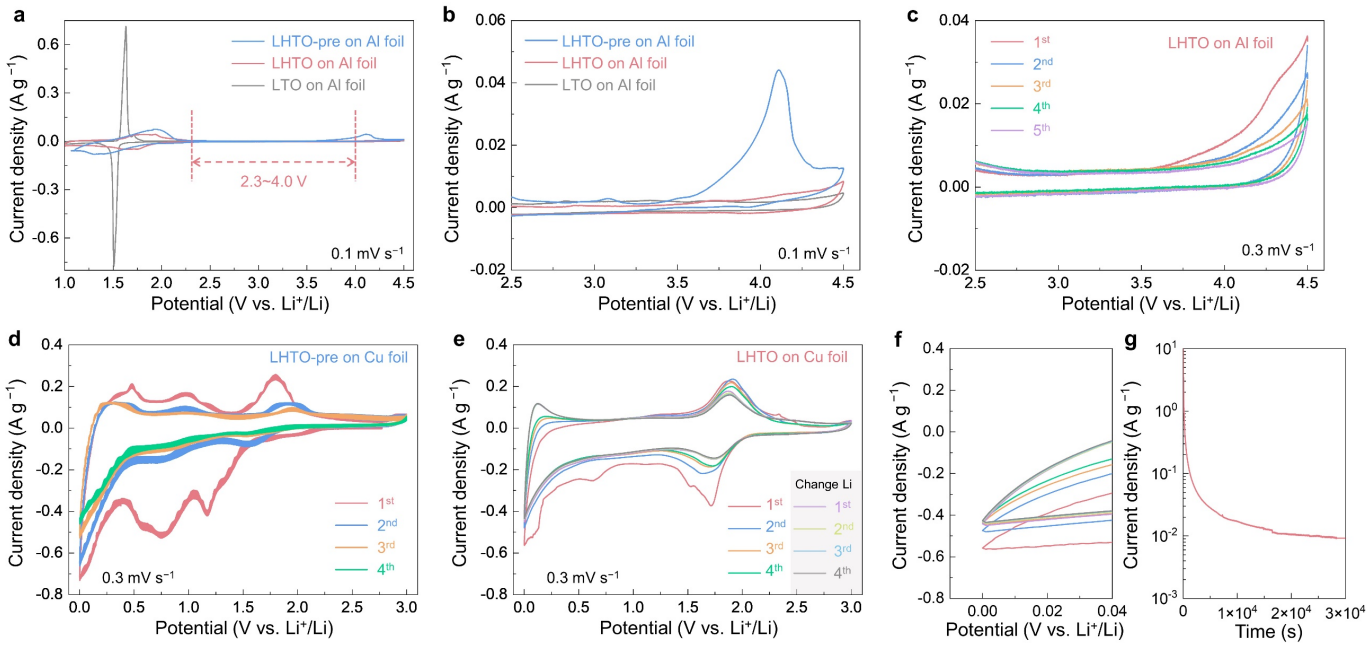

Figure 4. Electrochemical stability study of the synthesized Li-H-Ti-O quaternary compound. a, b) Scan cyclic voltammetry between 1.0~4.5 V at 0.1 mV s^{-1}, c) scan cyclic voltammetry between 1.0~4.5 V for 4 cycles at 0.3 mV s^{-1}. d~f) Scan cyclic voltammetry between 0.01~3.0 V at 0.3 mV s^{-1}. g) Polarization test at 0 V.

Since both LHTO-pre and LHTO contain confined water in their crystal structure, it remains a question how the confined water would affect their electrochemical stability. Here slow-scan cyclic voltammetry (CV) is performed to assess their electrochemical stability[27]. To examine the stability of these compounds at high potential, their powder is mixed with carbon and then cast onto an Al foil as an electrode. The electrode is then used as the working electrode in an Electrode|liquid electrolyte|Li cell for CV tests in 1.0~4.5 V vs Li^+/Li (**Figure 4**a). A pair of redox peaks is observed between 1.0~2.3 V for all three materials, which corresponds to the redox of Ti^{4+}/Ti^{3+}. If the Ti^{4+} is reduced to Ti^{3+}, the electronic conductivity will increase rapidly[28]. At above 2.3 V, an obvious peak appears for LHTO-pre starting from 3.5 V, which can be attributed to the oxidation of nano-confined water. In contrast, no clear redox peaks can be observed in 2.3~4.0 V for LHTO and LTO (Figure 4b). Besides the high-voltage stability, the reversibility for ionic transport should also be considered for a SE. After the first activation process, the curves from the 2nd to 5th cycles overlap quite well (Figure 4c), demonstrating the LHTO structure is quite stable at 1.0~4.5 V as an ionic conductor.

To examine their stability at low potential, their powder is mixed with carbon and then cast onto a Cu foil as the working electrode for CV tests in 0.01~3.0 V vs Li^+/Li (Figure 4d). For LHTO-pre, the CV (Figure 4d) shows several strong cathodic peaks during the first scan, which can be attributed to the reduction of absorbed water, nano-confined water, as well as the formation of solid electrolyte interface (SEI) on the surface of LHTO-pre (Figure S6, Supporting Information). The weakening of these peaks in the subsequent cycles suggests the formed SEI to some extent mitigate the further decomposition of the LHTO-pre. For LHTO, the reduction peaks during the first cycle are much weaker than those in LHTO-pre (Figure 4e, f), indicating the nano-confined pseudo-water is more stable than the nano-confined water. To examine if a stable SEI can form on the surface of LHTO, the cell is polarized to 0 V and the current response is recorded. After polarization for 20000 sec, the current decreases to below 10^{-2} A g^{-1}, which suggests the side reaction becomes negligible. It should be noted despite the LHTO being relatively stable at low potential, the reduction of Ti^{4+} renders it electronic-conductive and fails it as an SE. Therefore, similar to perovskite-type $Li_{3x}La_{2/3-x}\square_{1/3-2x}TiO_3$

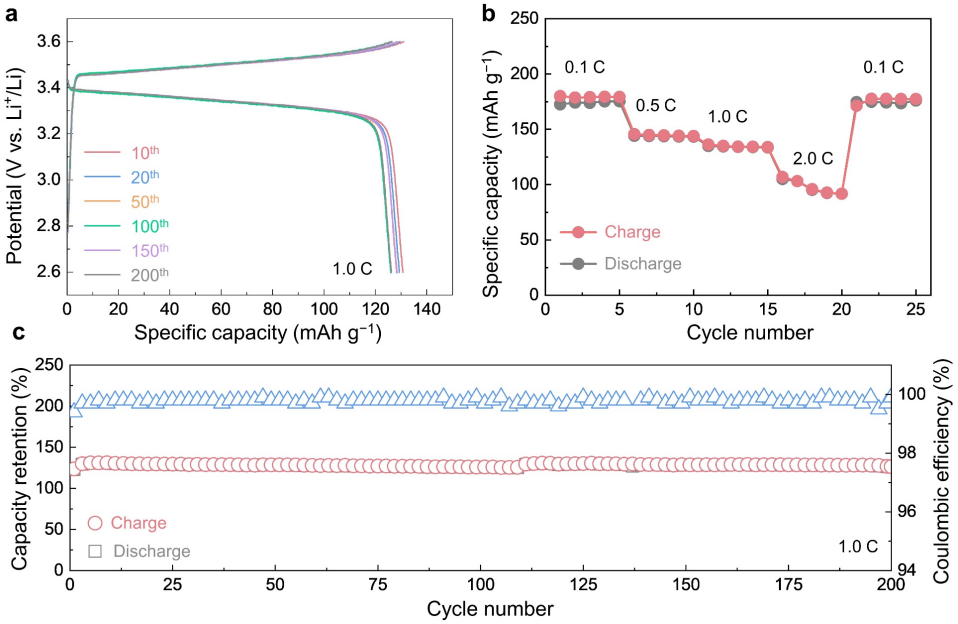

Figure 5. Electrochemical performances of LHTO in solid-state LIBs. a) Galvanostatic charge/discharge potential for different cycles at 1.0 C, b) rate capability, c) cycling performance at 1.0 C.

(LLTO)**,** an electronic insulator, e.g., polyethylene oxide (PEO), is still needed to avoid direct contact between Li metal and LHTO if it is used in a solid-state battery.

The above study suggests that LHTO could be used as the SE in a solid-state battery. To examine the performance of the synthesized LHTO compound as the SE in LIBs, $LiFePO_4$|LHTO|PEO|Li cells were assembled and tested at 60 ºC. The voltage curves during charging/discharging show a single plateau at ~3.45 V, and no redox behavior of Ti^{4+}/Ti^{3+} or decomposition of nano-confined pseudo-water can be detected, which demonstrates the feasibility of LHTO as the SE for solid-state LIBs (**Figure 5**a). Rate performance is further measured, and the results show the specific capacity at 0.1 C is close to the theoretical specific capacity of $LiFePO_4$ (170 mAh g^{-1}). With increasing current density, the specific capacity is 144 mAh g^{-1} at 0.5 C, and 135 mAh g^{-1} at 1.0 C (Figure 5b). Even at a high rate of 2.0 C, the battery can still deliver 58% of the theoretical specific capacity. Then the battery is cycled at 1.0 C for 200 cycles. The cell can retain 98% of its initial capacity at the 200^{th} cycle (Figure 5c). The Coulombic efficiency of the first cycle is 99.4%, and the average Coulombic efficiency during the 200 cycles is 99.8%. These results demonstrate that the LHTO can be used as a SE in solid-state LIBs.

3. Discussion

Several mechanisms could possibly explain the enhanced ionic transport in confined-water contained LHTO. First, confined water could shield the charge of Li-ion and decrease its migration barrier. In general, Li-ion hopping in oxides needs to break the strong Li–O ionic bond. Confined water can expand the bond distance from 1.948 Å to 1.969 Å for $Li^+(H_2O)_3$, and to 2.148 Å for $Li^+(H_2O)_6$[29], which can reduce the migration barrier. This phenomenon is called shielding effect[30], which has been observed to enhance ionic transport in electrode materials for various batteries, such as LIB, sodium-ion batteries, potassium ion batteries, Mg-ion batteries, and Zn-ion batteries (Table S3, Supporting Information). As a result, the Li-ion activation energy of LHTO-pre and LHTO can be decreased (more than 0.1 eV) compared to that of LTO (Figure 3b). Second, confined water leads to the formation of an amorphous-glassy phase, which could decrease the Li-ion migration barrier[25]. Braga *et al.* reported that the existence of H^+ was beneficial for the formation of an amorphous glassy phase, and very high ion conductivity of more than 10^{-2} S cm^{-1} was reported[31]. From the inset of Figure 2f, we have demonstrated the lattice distortion and disordered structure in $Li_{1.81}H_{1.13}Ti_2O_{5.15-\sigma}$, which could contribute to the ionic conductivity improvement. As a result, the Li-ion activation energy of LHTO can be further decreased (more than 0.2 eV) compared to that of LHTO-pre (Figure 3b).

For the enhanced electrochemical stability window of LHTO compared to LHTO-pre, the stronger covalent bonds in nano-confined pseudo-water could explain the enhanced electrochemical stability. Water is considered adverse to electrochemical applications due to its narrow electrochemical stability window (1.23 V)[32] and its incompatibility with aprotic electrolytes and metal anodes (e.g., Li metal)[33]. Whereas this traditional cognitive is challenged when water is well-confined **1)** in liquid electrolytes (well-known as "water-in-salts" electrolyte[34] or molecular crowding electrolyte[32]) or **2)** in electrodes. For **1)**, when a water molecule is confined by high-concentrated global/local salts, the electrochemical stability window can be expanded from 1.23 V (H_2O) or 2.0 V (traditional aqueous electrolyte), to 2.8 V (21 M LiTFSI), 3.0 V (19.4 M LiTFSI-8.3 M LiBETI) and 3.2 V (2 M LiTFSI-94%PEG-6%H_2O)[32] (Table S4, Supporting Information). For **2)**, when a water molecule is confined in the crystal structure of Ti-based, V-based, Mn-based electrodes, it can demonstrate 10^4~10^5 ultra-

stable cycling in aprotic electrolytes beyond the stable window of H_2O (Table S5, Supporting Information), such as 10000 stable cycles for $Li_{1.39}H_{1.18}Ti_2O_{5.29-\sigma}$ (1.0~2.5 V in LIB)[15], 8000 stable cycles for $Mn_{0.15}V_2O_5 \cdot nH_2O$ (0.2~1.7 V in zinc ion battery)[35], and 1000 stable cycles for $NaMnO_{2-y-\delta}(OH)_{2y}$ (2.0~4.0 V in sodium-ion battery)[36]. Therefore, we know that for three different types of water in water-containing oxides, the rank of them by activation energy under heat treatment is adsorbed water < nano-confined water < nano-confined pseudo-water. The sort orders of electrochemical treatment (electrochemical stability) are the same as that of heat treatment (thermal stability). The rank of Li-ion activation energy in an oxide framework is nano-confined pseudo-water < nano-confined water < one without water.

4. Conclusion

In conclusion, using the Li-H-Ti-O ternary compound as an example, it is demonstrated that the confined-water-containing compound shows 2~3 orders of magnitude enhancement in the Li-ion conductivity than water-free compound. The decomposition of nano-confined water narrows the electrochemical stability window of LHTO-pre, but the LHTO has the same electrochemical stability window as the water-free LTO. The enhanced ionic transport in these compounds is attributed to the reduced Li-ion migration barrier due to the shielding effect as well as the formation of the amorphous-glassy phase. The good stability window of LHTO can be attributed to the strong covalent bonds of the nano-confined pseudo-water. The performance of LHTO is further demonstrated in a solid-state battery ($LiFePO_4$|LHTO|PEO|Li), which shows excellent rate capability (58% rate retention at 2.0 C) and cyclability (200 stable cycles with 2% capacity loss). Such a discovery not only enhances Li^+ conductivity in Li-H-Ti-O solid electrolytes, but also opens a new avenue to tune the ionic conductivity of various oxides as solid electrolytes, such as Li-H-Zr-O, Li-H-Cl-O compounds. By controlling the amount, type, and location of the confined water in the oxides, new design freedom in tuning the properties of oxides, including but not limited to ion transport, is introduced, which opens a new avenue in designing novel ceramic materials for various applications.

5. Experimental Section

Materials synthesis: A typical preparation procedure of LHTO-pre consists of two steps. i) TiO_2 powder and concentrated NaOH solution were mixed and had a hydrothermal reaction at 150 °C for several hours, followed by ion substitution of Na^+ with H^+ in 0.5 M HNO_3 solution for several hours to obtain hydrogen trititanates (denoted as HTO). ii) For chemical lithiation, a certain concentration of LiOH solution and hydrogen trititanates were sealed into an autoclave and heated at 150 °C for 12 h. The hydrothermal product was washed with deionized water and dried at 70 °C, and the LHTO-pre powder was obtained. LHTO was obtained by a 2 h-thermal-treatment of LHTO-pre under vacuum at 200 °C.

Materials characterizations: TGA analysis was conducted on a thermogravimetric analyzer (STA 449F3) in flowing N_2 at 5 °C min^{-1} ramping rate from 50 °C to 500 °C. Chemical compositions were characterized by elemental analysis (EuroEA3000 elemental analyzer) for O and H, and by ICP-MS (IRIS Intrepid II XSP) for Li and Ti. FTIR spectra were obtained by Bruker spectrometer (VERTEX 70V) at 500~4000 cm^{-1}. XRD data were collected on Bruker D8 Advance X-ray diffractometer with Cu Kα (λ=0.154 nm). SEM images were taken on ZEISS microscopy (Gemini 2) and HRTEM images on JEOL microscopy (JEM-2100F).

Electrochemical characterizations: To measure the Li^+ and e^- conductivity, 120~200 mg powder material was pressed into a pellet (diameter 11 mm; thickness 600 μm) under pressure (~120 MPa) at 120 °C. DC measurements were conducted on a Zahner IM6 electrochemical workstation. A typical PEO-LITFSI film (EO/Li=20; thickness 100 μm) was used as a passive layer between the working pellet and lithium foil. A Li|PEO|pellet|PEO|Li cell was tested with an applied voltage of 0.1 V at different temperatures from 60 °C to 80 °C to acquire Li^+ conductivity and an ss|pellet|ss (ss refers to stainless steel) cell was used to test e^- conductivity. For evaluating the electrochemical stability window, the LHTO-pre/LHTO/LTO electrode slurry (powder: carbon black: polyvinylidene fluoride (PVDF) = 70:20:10) was cast onto the Al foil and Cu foil with average loading density of active materials of 1 mg cm^{-2}. The CV of Electrode|liquid electrolyte|Li cell (liquid electrolyte was 1 M $LiPF_6$ in EC: DC: EMC = 1:1:1 in volume) were tested at two potential window of 1.0~4.5 V and 0.01~3.0 V vs Li^+/Li. Ceramic-based film (thickness 60 μm) was used as the solid electrolyte to examine the performance of LHTO in LIB. LHTO powder, PVDF, and lithium bis(trifluoromethanesulfonyl)imide (LiTFSI) was mixed in N-methyl-2-pyrrolidinone solvent with a mass ratio of 65: 30: 5. The mixture was transferred to an open glass box and evaluated the solvent at 120 °C. Then roll squeezer was used to compact the obtained ceramic-based film. The solid LIBs were assembled into 2032-coin-type cells with LHTO ceramic-based film as solid electrolyte, commercial $LiFePO_4$ (20 wt% active material) as the working electrode, and lithium foil as a counter. A 5 μL liquid electrolyte was injected into the cathode side for moderating the LHTO/$LiFePO_4$ interface wettability. The galvanostatic charge-discharge tests at 60 °C of assembled Li|PEO|LHTO|$LiFePO_4$ cells were then conducted on LAND CT2001A battery analyzer between 2.6~3.6 V vs Li^+/Li.

Supporting Information

Supporting Information is available from the Wiley Online Library or from the author.

Acknowledgments

Y.L. and S.W. contributed equally to this work. Z.T. acknowledges support from the National Natural Science Foundation of China (No. 51772163 and No. 52172210). T.G. acknowledges the University of Utah for providing the start-up funding.

Conflict of Interest

The authors declare no conflict of interest.

Key words

solid electrolyte, confined water, conductivity, stability, Li-ion batteries

Received: ((will be filled in by the editorial staff))

Revised: ((will be filled in by the editorial staff))

Published online: ((will be filled in by the editorial staff))

References

[1] a) Y. Gao, A. M. Nolan, P. Du, Y. Wu, C. Yang, Q. Chen, Y. Mo, S. H. Bo, *Chem. Rev.* **2020**, 120, 5954; b) M. Li, C. Wang, Z. Chen, K. Xu, J. Lu, *Chem. Rev.* **2020**, 120, 6783; c) S. Randau, D. A. Weber, O. Kötz, R. Koerver, P. Braun, A. Weber, E. Ivers-Tiffée, T. Adermann, J. Kulisch, W. G. Zeier, F. H. Richter, J. Janek, *Nat. Energy* **2020**, 5, 259.

[2] W. Zhao, J. Yi, P. He, H. Zhou, *Electrochem. Energy Rev.* **2019**, 2, 574.

[3] Z. Zhang, Y. Shao, B. Lotsch, Y.-S. Hu, H. Li, J. Janek, L. F. Nazar, C.-W. Nan, J. Maier, M. Armand, L. Chen, *Energy Environ. Sci.* **2018**, 11, 1945.

[4] C. Wang, K. Fu, S. P. Kammampata, D. W. McOwen, A. J. Samson, L. Zhang, G. T. Hitz, A. M. Nolan, E. D. Wachsman, Y. Mo, V. Thangadurai, L. Hu, *Chem. Rev.* **2020**, 120, 4257.

[5] S. Chen, D. Xie, G. Liu, J. P. Mwizerwa, Q. Zhang, Y. Zhao, X. Xu, X. Yao, *Energy Stor. Mater.* **2018**, 14, 58.

[6] R. Kanno, T. Hata, Y. Kawamoto, M. Irie, *Solid State Ion.* **2000**, 130, 97.

[7] K. J. Kim, M. Balaish, M. Wadaguchi, L. Kong, J. L. M. Rupp, *Adv. Energy Mater.* **2020**, 11, 2002689.

[8] Y. Zhu, X. He, Y. Mo, *ACS Appl. Mater. Interfaces* **2015**, 7, 23685.

[9] C. E. Weaver, L. D. Pollard, *The chemistry of clay minerals*, Elsevier, **2011**.

[10] D. Zhang, C.-H. Zhou, C.-X. Lin, D.-S. Tong, W.-H. Yu, *Appl. Clay Sci.* **2010**, 50, 1.

[11] J. Kratochvíla, Z. Salajka, A. Kazda, Z. Kadlc, J. Souček, M. Gheorghiu, *J. Non. Cryst. Solids.* **1990**, 116, 93.

[12] R. Hafidz, C. Yaakob, I. Amin, A. Noorfaizan, *Int. Food Res. J.* **2011**, 18, 813.

[13] a) V. Augustyn, Y. Gogotsi, *Joule* **2017**, 1, 443; b) Y. Bahramian, A. Bahramian, A. Javadi, *Colloids Surf. A Physicochem. Eng. Asp.* **2017**, 521, 260; c) G. Hummer, J. C. Rasaiah, J. P. Noworyta, *Nature* **2001**, 414, 188; d) J. Khorami, A. Lemieux, *Thermochim. Acta* **1989**, 138, 97.

[14] H. D. Lutz, in *Solid Materials*, Springer Berlin Heidelberg **1988**, Ch. Chapter 3, p. 97.

[15] S. Wang, W. Quan, Z. Zhu, Y. Yang, Q. Liu, Y. Ren, X. Zhang, R. Xu, Y. Hong, Z. Zhang, K. Amine, Z. Tang, J. Lu, J. Li, *Nat. Commun.* **2017**, 8, 627.

[16] J. A. Darr, J. Zhang, N. M. Makwana, X. Weng, *Chem. Rev.* **2017**, 117, 11125.

[17] A. Feinle, M. S. Elsaesser, N. Husing, *Chem. Soc. Rev.* **2016**, 45, 3377.

[18] J. Proost, *J. Vac. Sci. Technol. B* **1998**, 16, 2091.

[19] J. Proost, M. Baklanov, K. Maex, L. Delaey, *J. Vac. Sci. Technol. B* **2000**, 18, 303.

[20] a) J. Texter, K. Klier, A. C. Zettlemoyer, in *Progress in Surface and Membrane Science*, Vol. 12 (Eds: D. A. Cadenhead, J. F. Danielli), Elsevier **1978**, p. 327; b) M. V. Vener, A. N. Egorova, A. V. Churakov, V. G. Tsirelson, *J. Comput. Chem.* **2012**, 33, 2303; c) S. A. Katsyuba, M. V. Vener, E. E. Zvereva, Z. Fei, R. Scopelliti, G. Laurenczy, N. Yan, E. Paunescu, P. J. Dyson, *J. Phys. Chem. B* **2013**, 117, 9094.

[21] H. G. Tompkins, *J. Vac. Sci. Technol. B* **1993**, 11, 727.

[22] B. A. Gaweł, A. Ulvensøen, K. Łukaszuk, B. Arstad, A. M. F. Muggerud, A. Erbe, *RSC Adv.* **2020**, 10, 29018.

[23] a) W. Kagunya, R. Baddour-Hadjean, F. Kooli, W. Jones, *Chem. Phys.* **1998**, 236, 225; b) X. Wang, Z. Li, D. Y. Wu, G. R. Shen, C. Zou, Y. Feng, H. Liu, C. K. Dong, X. W. Du, *Small* **2019**, 15, e1804832.

[24] M. Wang, N. R. Jaegers, M. S. Lee, C. Wan, J. Z. Hu, H. Shi, D. Mei, S. D. Burton, D. M. Camaioni, O. Y. Gutierrez, V. A. Glezakou, R. Rousseau, Y. Wang, J. A. Lercher, *J. Am. Chem. Soc.* **2019**, 141, 3444.

[25] a) C. A. Angell, *Solid State Ion.* **1983**, 9-10, 3; b) J. Fu, *J. Am. Ceram. Soc.* **2005**, 80, 1901; c) X. Xu, Z. Wen, X. Wu, X. Yang, Z. Gu, *J. Am. Ceram. Soc.* **2007**, 90, 2802.

[26] R. Chen, Q. Li, X. Yu, L. Chen, H. Li, *Chem. Rev.* **2020**, 120, 6820.

[27] F. Han, Y. Zhu, X. He, Y. Mo, C. Wang, *Adv. Energy Mater.* **2016**, 6, 1501590.

[28] X. Chen, L. Liu, F. Huang, *Chem. Soc. Rev.* **2015**, 44, 1861.

[29] T. M. Alam, D. Hart, S. L. Rempe, *Phys. Chem. Chem. Phys.* **2011**, 13, 13629.

[30] a) M. Mao, T. Gao, S. Hou, C. Wang, *Chem. Soc. Rev.* **2018**, 47, 8804; b) G. Fang, J. Zhou, A. Pan, S. Liang, *ACS Energy Letters* **2018**, 3, 2480; c) M. Song, H. Tan, D. Chao, H. J. Fan, *Adv. Funct. Mater.* **2018**, 28, 1802564; d) F. Wu, H. Yang, Y. Bai, C. Wu, *Adv. Mater.* **2019**, 31, e1806510; e) F. Ambroz, T. J. Macdonald, T. Nann, *Adv. Energy Mater.* **2017**, 7, 1602093.

[31] a) M. H. Braga, A. J. Murchison, J. A. Ferreira, P. Singh, J. B. Goodenough, *Energy Environ. Sci.* **2016**, 9, 948; b) M. H. Braga, N. S. Grundish, A. J. Murchison, J. B. Goodenough, *Energy Environ. Sci.* **2017**, 10, 331.

[32] J. Xie, Z. Liang, Y. C. Lu, *Nat Mater* **2020**, 19, 1006.

[33] T. Kawamura, S. Okada, J.-i. Yamaki, *J. Power Sources* **2006**, 156, 547.

[34] a) L. Suo, O. Borodin, T. Gao, M. Olguin, J. Ho, X. Fan, C. Luo, C. Wang, K. Xu, *Science* **2015**, 350, 938; b) L. Suo, Y. S. Hu, H. Li, M. Armand, L. Chen, *Nat. Commun.* **2013**, 4, 1481.

[35] H. Geng, M. Cheng, B. Wang, Y. Yang, Y. Zhang, C. C. Li, *Adv. Funct. Mater.* **2019**, 30, 1907684.

[36] H. Xia, X. Zhu, J. Liu, Q. Liu, S. Lan, Q. Zhang, X. Liu, J. K. Seo, T. Chen, L. Gu, *Nat. Commun.* **2018**, 9, 5100.